

Properties of nanoparticles affecting simulation of fibrous gas filter performance

*Original*

Properties of nanoparticles affecting simulation of fibrous gas filter performance / Tronville, PAOLO MARIA; Rivers, R.. - In: JOURNAL OF PHYSICS. CONFERENCE SERIES. - ISSN 1742-6596. - ELETTRONICO. - 617:(2015), pp. 1-10. [10.1088/1742-6596/617/1/012010]

*Availability:*

This version is available at: 11583/2608777 since: 2016-09-25T19:05:08Z

*Publisher:*

IOP Publishing

*Published*

DOI:10.1088/1742-6596/617/1/012010

*Terms of use:*

This article is made available under terms and conditions as specified in the corresponding bibliographic description in the repository

*Publisher copyright*

(Article begins on next page)

## Properties of nanoparticles affecting simulation of fibrous gas filter performance

This content has been downloaded from IOPscience. Please scroll down to see the full text.

2015 J. Phys.: Conf. Ser. 617 012010

(<http://iopscience.iop.org/1742-6596/617/1/012010>)

View [the table of contents for this issue](#), or go to the [journal homepage](#) for more

Download details:

IP Address: 130.192.33.177

This content was downloaded on 31/05/2015 at 14:49

Please note that [terms and conditions apply](#).

## Properties of nanoparticles affecting simulation of fibrous gas filter performance

Paolo Tronville<sup>1</sup>, Richard Rivers<sup>2</sup>

<sup>1</sup> Politecnico di Torino DENERG, Corso Duca degli Abruzzi, 24 10129 Turin, Italy

<sup>2</sup> EQS, Inc. 1262 Bassett Ave. Louisville, Kentucky 40204 USA

E-mail: paolo.tronville@polito.it

**Abstract.** Computational Fluid Dynamics (CFD) codes allow detailed simulation of the flow of gases through fibrous filter media. When the pattern of gas flow between fibers has been established, simulated particles of any desired size can be “injected” into the entering gas stream, and their paths under the influence of aerodynamic drag, Brownian motion and electrostatic forces tracked. Particles either collide with a fiber, or pass through the entire filter medium. They may bounce off the fiber surface, or adhere firmly to the surface or to particles previously captured. Simulated injection of many particles at random locations in the entering stream allows the average probability of capture to be calculated. Many particle properties must be available as parameters for the equations defining the forces on particles in the gas stream, at the moment of contact with a fiber, and after contact. Accurate values for all properties are needed, not only for predicting particle capture in actual service, but also to validate models for media geometries and computational procedures used in CFD. We present a survey of existing literature on the properties influencing nanoparticle dynamics and adhesion.

### 1. Introduction

The immense growth of nanotechnology in recent years means that nanoparticles will appear in industrial and research locations at levels which demand careful air pollution control. Vehicular exhausts pollute the air in cities and along highways with unacceptable aerosol concentrations, including nanoparticles. It is important to understand and quantify the details of nanoparticle by fibrous filters, to promote the development of effective, reliable and minimum-cost solutions to nanoparticle filter systems design.

The authors have previously discussed the effect of nanofiber additions to air filter media [1]. The present paper is concerned with the physical properties of nanoparticles which affect their capture and build-up in fibrous air filters, regardless of the characteristics of the fibers in the filter media.

Several studies found in our literature review had a recurring theme: the behavior of instruments based on “classic” concepts cannot necessarily be extended to aerosol particles with low-nanometer sizes. Flow patterns in differential mobility analyzers that appear unimportant for micrometer-sized particles may affect results for nanoparticles. Particle-charge neutralization in bipolar ion fields are not described by the same expressions for nanoparticles as for larger particles. Particle count devices may have very different count efficiencies for particle sizes above and below 100 nm. Agglomeration of fundamental nanoparticles can confuse results.



## 2. Nanoparticle properties of interest to filtration simulation

Properties of aerosol particles which must be known for CFD simulations are:

- Form and size distribution;
- Aerodynamic drag as a function of size and form;
- Density, both of simple forms and agglomerates;
- Count in a sample or sample flow;
- Bounce;
- Adhesion properties, both to filter media fibers and to other particles of their own kind;
- Diffusion parameters;
- Electrical charge distributions as a function of size and neutralizer properties;
- For liquid particles, evaporation rates.

Tests of the validity of CFD simulations are, ultimately, the accuracy with which a CFD model and calculation procedure duplicates experimental data on the filter media simulated. Incorrect property values lead to meaningless simulations.

### 2.1. Forms of nanoparticles

Nanoparticle can have relatively simple geometries, such as spheres, cubes, cylindrical rods. Platelet forms – thin round discs or flat polygons, exist. Agglomerates with maximum dimensions below 100 nm – the usual definition of nanoparticles – are commonplace, since they are created in flames and by both spark-ignition and diesel engines. Such aggregates consist of smaller primary nanoparticles, but for filtration studies, aggregates must be considered as single, though complex, forms. Nanoparticles of carbon have some of the most exotic forms: hollow quasi-spherical “fullerenes”; single or multilayer hollow nanotubes; spirals. Gel nanoparticles can exist in spherical or ellipsoidal form.

The behavior of a non-spherical particle is often expressed in terms of the diameter of a sphere having like behavior. Unfortunately, the equivalent spherical diameter depends on the specific effect or property considered. Figure 1 shows five equivalent diameters for a relatively simple hexagonal platelet particle.

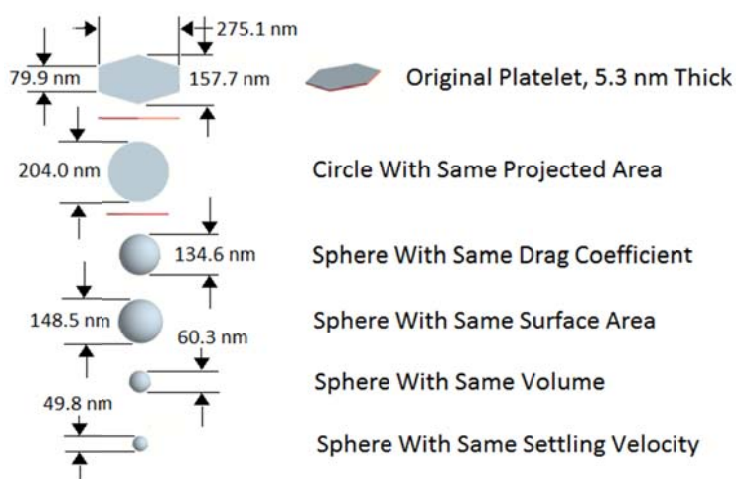


**Figure 1.** Circle and sphere equivalents to a hexagonal platelet (Adapted from [2])

Shape, size and density are especially difficult to define for an agglomerate. One needs to know the number and dimensions of its fundamental particles, often rather uniform spheres of low nanometer diameter. Other dimensions of its size and structure are needed: maximum length and width, and the *radius of gyration* of the agglomerate. With these, a quantitative measure of the agglomerate complexity, its *fractal dimension*, can be calculated. For aerosol agglomerates, this can often be

determined by analysis of two-dimensional electron microscope images using computer algorithms. Rogak, Flagan and Nguyen [3] provide a description of these image-analysis procedures. An approximation to the fractal dimension is a simple function of the number of primary particles in an agglomerate and square root of the product of the particle's length and width (Sander [4]). Examples of agglomerate characterization are given in Patterson and Kraft [5]. Useful explanations of the terminology in that paper and others which make use of fractal concepts are given on two internet sites [6] and [7].

Several studies have taken a somewhat different approach to establishing the fractal dimension and fractal prefactor of aggregates. Assuming or calculating the size and size distribution of primary particles, and fractal dimension and fractal prefactor values, they generate large numbers of images of aggregates. Various models of the agglomeration physics are possible. These simulated images frequently match the appearance of TEM or SEM images of the agglomerates studied quite well, indicating that the parameter choices were appropriate. [8] and [9] discuss ways in which the agreement between simulations and measurements can be quantified, and in particular, the best means to obtain reliable fractal descriptions of 3D agglomerates from 2D images.

### 2.2. Size distributions of nanoparticles

Many studies have shown that primary nanoparticles can exist as essentially uniform particles. More often, however, the size distributions are log-normal. The same mathematical relationships and graphical representations that are used with micrometer-scale particles apply to distributions at nanometer scale. Simple particle forms have a characteristic dimension, which for a cloud of particles can have a size-dependent distribution. Sodium chloride particles, for example are frequently cubical, characterized by the length of a side; cylindrical particles can have size distributions for both diameter and length. Agglomerates can have wide size ranges, but no easily defined size, hence no easily specified size. What can be defined and measured for agglomerates are their mobilities, aerodynamic, diffusive and electrical. Mobility is defined as: [particle velocity relative to local gas velocity] / [force on particle].

The term [force on particle] is different for aerodynamic, diffusive, and electrical mobility. These three forces and means for measuring them are discussed in sections below. Because agglomerates have no definable size, their size distributions are often stated in terms of some "equivalent mobility diameter", dependent on the method used to obtain the distribution. An alternative "size" is some measurable geometric value, obtained from SEM images. One example of SEM-measured size is the determination of the smallest rectangle able to enclose the particle. Image-analysis software packages, both commercial and open-source, are available to measure such dimensions more or less automatically, and characterize the distributions of them.

### 2.3. Aerodynamic drag of nanoparticles

The aerodynamic drag  $\mathbf{F}_{\text{drag}}$  of a sphere with low Reynolds number moving in a gas stream is given by Stokes law with the Cunningham correction:

$$\mathbf{F}_{\text{drag}} = 3\pi\mu d_p (\mathbf{u}_g - \mathbf{u}_p) \cdot (m_p C_c)^{-1}$$

Where  $\mu$  = gas dynamic viscosity;  $d_p$  = sphere diameter;  $\mathbf{u}_g$  = gas velocity;  $\mathbf{u}_p$  = particle velocity;  $m_p$  = particle mass; and  $C_c$  = Cunningham's correction for slip at the particle surface, a function of gas type, temperature and pressure. With  $\lambda$  = gas mean-free-path and Knudsen Number defined as

$$Kn = 2\lambda (d_p)^{-1}$$

$$C_c = 1 + Kn(A + B \exp(-C_c / Kn))$$

This classic relationship has been shown [10] to hold for particles as small as 0.012 times the mean free path of the gas molecules. [10] provides  $A$ ,  $B$ , and  $C$  for dry air. Since the expression for  $C_c$  is a function of Knudsen Number, the values of  $A$ ,  $B$ , and  $C$  should be applicable to any gas and set of test conditions for which the mean-free path of the gas and the particle diameter are known.

Tammet [11] demonstrates that modifications to the expression for the Cunningham correction in [10] are needed for spheres with diameters below 4 nm. His correction is added to the values of  $d_p$  wherever they appear in the Cunningham correction, including the values for  $Kn$ , and also in the above expression for aerodynamic drag  $F_{\text{drag}}$ .

If an airflow containing aerosol particles is passed through a properly dimensioned sequence of circular orifices, the aerosol particles are confined to a narrow beam, which expands in the region downstream of the last orifice. A typical pattern of flow through such an “aerodynamic lens” is shown in figure 2, from [12]. CFD calculations compared to the measured angular dispersion of the aerosol beams and the fraction of particles passing completely through the lens provide sensitive tests of both the expression for aerodynamic drag and the parameters values used in the CFD calculations.

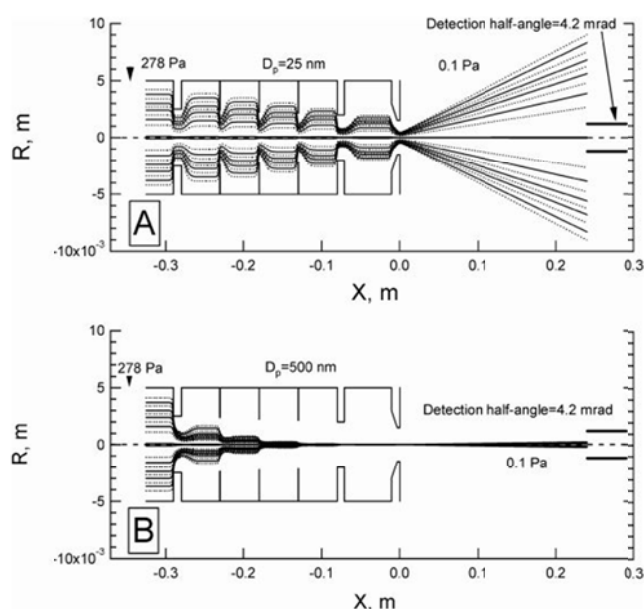


**Figure 2.** CFD-Simulated particle paths through an aerodynamic lens.  
A: 25 nm diameter particle;  
B: 500 nm diameter particle  
( from Zhang [12 ])

It is, however, important to include the effect of Brownian motion in the simulation. Reference [13] discusses the combined effects of aerodynamic drag and Brownian motion on aerodynamic lens performance for nanoparticles. The net result of these studies appears to be that the theory-based expressions for aerodynamic drag and Brownian motion are reliable, provided “slip” of gas molecules at the particle surface is properly included (also cf. Lewis [14]).

Some particles approaching an aerodynamic lens will strike the surface surrounding the entrance orifice. Other particles will strike the walls of the chambers and the orifices inside the lens. The fraction of entering particles which reaches the lens outlet can be calculated by CFD, and compared to measured values. Liu et.al. [15] reporting such comparisons, conclude that the agreement between simulation and measurement validates the parameter values and equations used for simulation. Sorensen [14] reviews the extensive literature on determination of the “mobility radius” of agglomerates, which is the radius of a sphere having the same aerodynamic drag as the agglomerate. He covers the entire range of particle Knudsen Numbers, hence nanoparticles.

#### 2.4. Density of nanoparticles and agglomerates

Density is mass divided by volume. For analyses of particle capture in fibrous filtration “volume” may not be the volume of the fundamental material making up the particle, but the volume which defines its

aerodynamic drag. For relatively simple nanoparticle forms, it may be possible to determine particle volume from SEM images, but masses cannot be determined gravimetrically.

The mass of aerosol particles can be measured with a single device, the Aerosol Particle Mass Analyzer (APM) making use of two properties of the particle simultaneously. The APM injects particles into the gap between two rotating cylinders. The gas in this gap rotates, imparting a centripetal force on the particle, proportional to its mass. This force is balanced by an electrostatic field established between the cylinders acting on a known charge on the particle. Figure 3a shows the design of the design of the APM, and figure 3b the equations which allow the calculation of the mass of the particle.

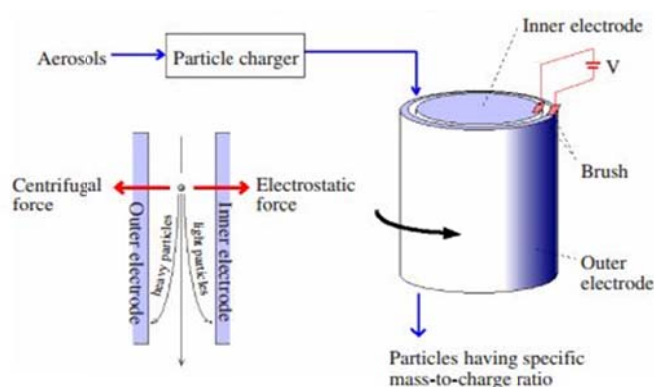


**Figure 3a.** Aerosol Particle Mass Analyzer Concept (from Kanomax APM Operation Manual)

$$mr\omega = q \frac{V}{r \cdot \ln(r_o/r_i)}$$

where  $m$  = particle mass  
 $\omega$  = angular rotation speed  
 $r$  = particle location relative to axis of rotation  
 $q$  = particle charge  
 $r_i$  = radius of inner electrode  
 $r_o$  = radius of outer electrode  
 $V$  = applied voltage

**Figure 3b.** APM Force Balance Equation (after Kanomax APM Operation Manual)

The density of nanoparticles can also be determined by pairs of instruments which allow extraction of the density value. A common pair is the differential mobility analyzer (DMA) and the vacuum aerodynamic particle sizer. An extensive review of non-spherical aerosol particle density measurement methods is given in [15].

### 2.5. Bounce properties of nanoparticles

Most early studies of particle bounce were made for the configurations present in single impactors and cascade impactors. A few metal-fiber filter forms exist, and for these the impactor studies are relevant. The impactor substrates studied rarely bear any resemblance to the common fibers in fibrous filter media, which are now formed of glasses, ceramics, synthetic organic polymers or natural organic materials like cotton (cellulose) or animal hairs (proteins). In addition, impactor substrates are often coated with greases or oils, or wetted, specifically to eliminate particle bounce. Such coatings are rare in fibrous filtration.

Several studies have attempted to quantify particle bounce from the fundamentals of elastic-body mechanics. [16], [17], [18] and [19] are among those who have taken this approach. Sato, Chen and Pui [20] extend these concepts to nanoparticles, and consider adhesion and removal effects as well.

### 2.6. Adhesion properties of nanoparticles

In general, adhesion forces binding particles to surfaces become stronger as particle size decreases, the forces of removal by aerodynamic drag become smaller for decreasing size, and bombardment by other particles becomes less probable. Thus re-entrainment of nanoparticles from filter fibers is minimal. Still, re-entrainment can occur. The theoretical aspects of adhesion forces are discussed in [21] and [22]. Extensive treatments of many aspects of particle adhesion are given in [23]. Remarkable adhesion effects resulting from high-energy collisions of nanoparticles with surfaces are described in [24]. A series of slides illustrating the complexity of particle adhesion is given at the website [25].

### 2.7. Diffusion of nanoparticles in filtration

In filtration, the diffusion process of interest is Brownian motion, the erratic path taken by particles as a result of unbalanced impacts from the molecules of the gas surrounding the particle. The (vector) acceleration of a particle can be defined as the sum of the (vector) aerodynamic drag force per unit mass and the (vector) Brownian force per unit mass:

$$\frac{d^2\mathbf{V}}{dt^2} = \mathbf{F}_D + \mathbf{F}_B$$

The aerodynamic drag on the particle is the “classic” definition described above, with the Cunningham correction  $C_C$  using a value of  $Kn$  appropriate for the nanoparticle size. To simulate Brownian motion, one must create a series of randomly directed forces at random time intervals. The power spectrum of these forces must have a Gaussian distribution, and must have an average power level  $S_{nn}$  given by

$$S_{nn} = kTC_C / (3\pi\mu d_p)$$

The time of application of each Brownian impact is randomized, as is its spatial direction. This procedure produces the erratic pattern characteristic of Brownian motion, superimposed on the general direction of particle motion resulting from  $\mathbf{F}_D$ .

### 2.8. Nanoparticle charging and neutralization

The unipolar charging of nanoparticles has been studied extensively, chiefly in connection with electrostatic precipitators and to support the interpretation of data from instruments that make use of charging to measure particle size and density. Charged aerosols are more easily captured by fibrous filters, whether or not they have electret properties or externally applied electrostatic fields. But charging aerosols to improve fibrous filter efficiency is dangerous, for if the capture efficiency somehow declines, the charged particles pass into the downstream space, and the charged particles precipitate rapidly on surfaces in the space, even forming visible patterns.

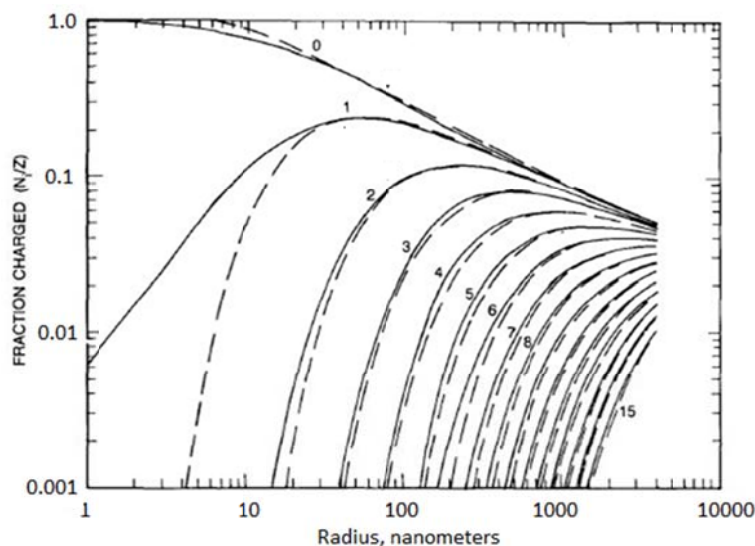


**Figure 4.** Probability of  $N$  elementary charges per particle on an aerosol at Boltzmann equilibrium, i.e. “neutralized”. (From Hoppel and Frick [27]. Dashed curves follow Fuchs [26])

Unipolar charging is used to neutralize aerosols which carry high unipolar charges as a result of their generation method. Bipolar charging - the exposure of an aerosol to a cloud of mixed positive and negative ions - is important to aerosol experimentation in many ways. Knowledge of charge distributions on aerosols is also critical for simulation of particle capture in fibrous filtration. The probable number of charges on each diameter of particle needs to be known. An electrostatically



“neutral” aerosol cloud is not charge-free; each individual particle in the cloud carries some number of elementary charges, ranging from zero to  $N$  elementary charges, either positive or negative. For an aged aerosol, the Boltzmann equilibrium distribution will be approached. Aerosols freshly generated in the laboratory are passed through clouds of mixed positive and negative ions to reach equilibrium quickly. The ion-production devices of such neutralizers can depend on radioactive sources (Kr-85 or Po-210), soft X-rays, or high-voltage corona discharge to produce the bipolar ion clouds needed. Covert, Wiedensohler and Russell [26] critique neutralizing devices. Like so many things in aerosol experimentation, care in choosing a neutralizer adequate for the conditions of an experiment is essential.

Fuchs [27] developed the basic form of the distribution of charges on aerosols exposed to a balanced bipolar ion cloud (one with equal numbers of positive and negative ions). Hoppel and Frick [28] extended the analysis to nanometer-size particles, and provided plots of the Boltzmann equilibrium distribution of charge on particles with radii 1 nm to 4  $\mu\text{m}$ . Stommel and Riebel [29] found errors in these earlier works, and provide corrections. The limited results of their corrections deviate slightly from the plot from Hoppel and Frick (figure 4).

### *2.9. Evaporation of liquid nanoparticles*

The literature on nanoparticle evaporation is chiefly related to high-temperature evaporation of metal particles. Li and Davis [30] conducted experiments on evaporation of dibutyl-phthalate particle evaporation in air at pressures decreasing from 13.7 kPa to 0.016 kPa. Their results are expressed as evaporation rates as a function of Knudsen Number, so may be applicable to nanoparticles at normal pressures. Their experimental conditions involved values of  $Kn$  as high as 2. Sutter et.al. [31] studied the evaporation of n-hexadecane particles with mass-mean diameters as small as 1.5  $\mu\text{m}$  actually on filter fibers. Evaporation rates were substantially lower than predicted by traditional mass-transfer theory (Fick’s Law). The mass of nanoparticle aerosols is very small, so evaporation may not result in appreciable health hazards.

### *2.10. Counting of nanoparticles for filtration studies*

Light-scattering aerosol spectrometers, widely used for counting particles of micrometer dimensions, have lower detection limits of about 90 nm, hence limited application in nanoparticle studies.

Nanoparticles can be examined by a transmission electron microscope (TEM) or scanning electron microscope (SEM), and the number of particles counted. Nuclear track-etched polycarbonate membrane filters provide a relatively featureless image background, allowing some automation of the counting process when SEM images are obtained. Preparation of nanoparticle samples for these imaging processes is more difficult than for light microscopy; the samples must be given a thin conductive coating, usually of a gold/palladium alloy, in an ion sputtering device.

Image-analysis computer programs are available to assist the particle counting process, including an open-source one (fracpac, an add-on for imagej). Electron microscope imaging is essentially the reference method for evaluating all other devices used to study aerosol particle geometry. It avoids the assumptions about particle charging, aerodynamic drag and diffusion effects necessary for interpreting the results of data from instruments such as the MOUDI, ELPI, DMA, SMPS, and APM.

The usual device for nanoparticle counting in gas flows is the condensation particle counter (CPC), which increases the size of individual particles by condensing a vapor onto them, then counting the enlarged particles by light-scattering. While the counting efficiency of a CPC is not 100% for all size particles, the efficiency values are reasonably stable and predictable, and useful counts can be obtained for particles below 10 nm diameter. The accuracy of results decreases as the size detected decreases.

Particle capture efficiency measurements for filter media require simultaneous upstream and downstream sampling, or very stable aerosol generation. In addition, it is essential that the sampling systems upstream and downstream, and the two flow rates, be as nearly identical as possible, so that particle losses in the two sampling systems are the same.

### 3. Generation of nanoparticles for filtration studies

Biskos et.al.[32] provide descriptions of the many ways available for nanoparticle generation. They discuss the potential of several methods to yield compact aerosol forms, rather than agglomerates, and provide an extensive bibliography for the details of various methods. Here we comment on some of the available generation methods.

Tiwari, Fields and Marr [33] dispersed dry nanoparticle powders using the generator described in [34]. The nanoparticle powders must be produced in some way which provides high yields of particles with defined properties. Powders of many substances are commercially available.

Liquid dispersions of nanoparticles can be diluted with ultrapure water, aerosolized by spraying, then passed through an evaporator to create individual spherical nanoparticles. Dispersions of polystyrene latex, gold and silver with certified diameters and standard deviations are available commercially with diameters as small as 1 nm. Raabe [35] gives the dilution needed to yield a given fraction of single particles in each spray droplet, depending on the droplet size distribution. Sheehan et.al. [36] generated nanoparticles by creating solution droplets with a Collison atomizer, stripping the larger particles with a cyclone, then evaporating the droplet water. Using an electrospray, instead of more conventional atomizers, gives smaller droplets, increasing the chance of dispersing individual particles. Electrosprayed droplets can also be solutions which evaporate to yield individual nanoparticles whose shape depends on the nature of the solute [37]. Figure 5 shows such a generator, which incorporates a bipolar ion source to neutralize the aerosol, which would otherwise be highly charged.

A popular means of generating liquid nanoparticles is to evaporate a liquid, then condense its vapor. Metals, such as gold and silver, can also be vaporized if high enough temperatures are available. Ji et.al. [38] describe such a generator. A widely-used means to reach temperatures high enough to vaporize metals is spark-discharge, Meuller et.al. [39] review controlled spark-discharge nanoparticle generation.

Flames can of course produce carbon nanoparticle agglomerates in the laboratory, as they do in the outdoor environment. They also produce occasional fullerene-structure particles. For filter media testing, steady aerosol generation rates with substantial particle counts are needed. Means to generate all fullerene forms – single – and multiple-wall nanotubes, “buckyballs”, spirals – have all been developed. The methods are employed for carbon nanoparticle generation, and many other materials, include laser ablation, spark generation; and furnace, flame, plasma and laser-stimulated reactors. These last four methods allow the creation of nanoparticles of selected chemical composition, especially organic compounds and metal oxides. Flows of *precursor compounds* are provided, either in solution or as gases, then passed into zones where energy is injected. The addition of substantial energy produces the reactions needed to create the desired compounds. A cooling zone is provided; there the hot vapors condense into particles. Sometimes an additional hot zone is provided for melting or *sintering* any agglomerates present into compact particles. Figure 6 shows a generator using a flame to oxidize a feed flow of liquid aerosol precursor particles. The mix of combustion and inert gases, and the form of the flame, provide conditions which optimize the yield of nanoparticles, either in primary form or as agglomerates as desired [40].

Iida et.al. [41] generated particles with diameters as small as 300 nm using an ink-jet generator; it seems possible to do the same with vibrating orifice generators, such as described by Mitchell, Snelling and Stone [42].

Wang and Tronville examined nanoparticle generation methods for their suitability to adaption as standardized test methods [43].

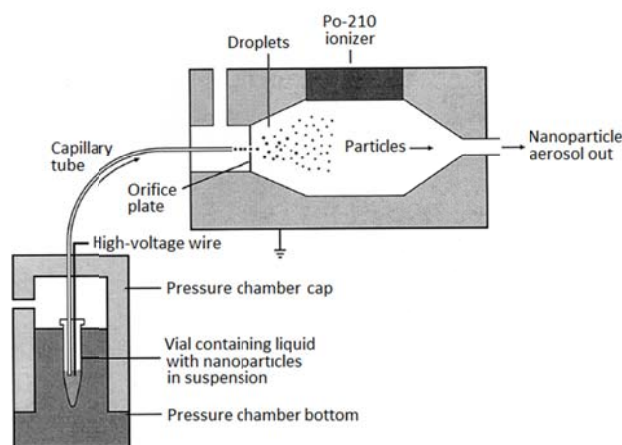


**Figure 5.** Electro-spray nanoparticle generator (modified from TSI catalog illustration)

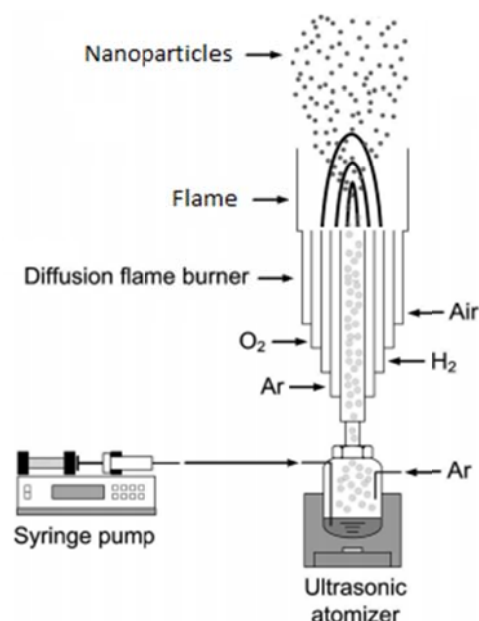


**Figure 6.** Flame spray pyrolysis generator (modified from Cho et al. [38])

## References

- [1] Zhou B, Tronville P, Rivers R 2013 *HVAC&R Research* **19** 503–512
- [2] Gallego-Urrea J A, Hammes J, Cornelis G and Hasselov M 2014 *J. Nanopartical Res.* **16** 2383–2400
- [3] Rogak S N, Flagan R C and Nguyen H V 1993 *Aerosol Sci. & Tech.* **18** 25–47
- [4] Sander M, Patterson R I A, Raj A and Kraft M 2009 On the fractal dimension of soot particles Cambridge Centre for Computational Chem. Eng. *Preprint* 80
- [5] Patterson R I A and Kraft M 2007 *Combustion and Flame* **151** 160–172
- [6] fractalfoundation.org
- [7] imagej.nih.gov/ij/plugins/fraclac
- [8] Chakrabarty R K, Garro M A, Garro R A, Chancellor S, Moosmütter H and Herald C M 2011 *Aerosol Sci. & Tech.* **45** 75–80
- [9] Chakrabarty R K, Garro M A, Garro R A, Chancellor S, Moosmütter H and Herald C M 2011 *Aerosol Sci. & Tech.* **45** 903–908
- [10] Kim J H, Mulholland G W, Kukuck S R and Pui D Y H 2005 *J. Res.National Inst. Standards and Tech.* **110** 31–54
- [11] Tammet H 2012 *Aerosol Sci. & Tech.* **46** i–iv
- [12] Zhang X F, Smith K A, Worsnop D R, Jiminez J L, Jayne J T, Kolb C E, Morris J and Davidovits P 2004 *Aerosol Sci. & Tech.* **38** 619–638
- [13] Wang X L, Kruis F E and McMurry P H 2005 *Aerosol Sci. & Tech.* **39** 624–636
- [14] Lewis E R 2010 *J. Aerosol Sci.* **41** 418–25
- [15] Liu P S K et.al. 2007 *Aerosol Sci. & Tech.* **41** 721–733
- [16] Sorensen C M 2011 *Aerosol Sci. & Tech.* **45** 765–779
- [17] DeCarlo P F, Slowik J G, Worsnop D R, Davidovits P and Jiminez J L 2004 *Aerosol Sci. & Tech.* **38** 1185–1205
- [18] Dahneke B 1975 *J. Colloid Interface Sci.* **51** 58–65
- [17] Tsai C J, Pui D Y H and Liu B D Y H 1990 *Aerosol Sci. & Tech.* **12** 497–507
- [18] Dunn P F, Brach R M and Janson G G 1996 *Aerosol Sci. & Tech.* **25** 445–465

- [19] Brach R M and Dunn P F 1998 *Aerosol Sci. & Tech.* **29** 379–388
- [20] Sato S, Chen D R and D.Y.H. Pui D Y H 2007 *Aerosol and Air Quality Res.* **7** 278–303
- [21] Carrillo J Y, Raphael E and Dobrynin A V 2010 *Langmuir* **26** 12973–12979
- [22] Thomas J 2003 Mechanics of nanoparticle adhesion – a continuum approach. *Particles on Surfaces* ed K.L. Mittal (New York: Marcel Dekker) Chap. 8
- [23] Mittal K L and Jaiswal R 2015 *Particle Adhesion and Removal* (New York: Wiley)
- [24] Suri M and Dumitrica T 2008 *Phys. Rev. B* **78** 081405
- [25] web2.clarkson.edu/projects/crcd/me537/downloads/slides/Rimai.pdf
- [26] Covert D, Wiedensohler A and Russell L 1997 *Aerosol Sci. & Tech.* **27** 206–214
- [27] Fuchs N 1963 *Geofis. Pura Appl.* **56** 185–192.
- [28] Hoppel W and Frick G 1990 *Aerosol Sci. & Tech.* **12** 471–496
- [29] Stommel Y G and Riebel U 2007 *Aerosol Sci. & Tech.* **41** 840–847
- [30] Li W G and Davis E J 1996 *Aerosol Sci. & Tech.* **25** 11–21
- [31] Sutter B, Bémer D, Appert-Collin J C, Thomas D and Midoux N 2010 *Aerosol Sci. & Tech.* **44** 394–404
- [32] Biskos G, Vons, V, Yurteri C U and Schmidt-Ott A 2008 *KONA Powder & Particle J.* **26** 13–35
- [33] Tiwari A J, Fields C G and Maur L C 2013 *Aerosol Sci. & Tech.* **37** 1267–1275
- [34] Tang P, Fletcher D F, Chan H K and Raper J A 2008 *Powder Tech.* **187** 27–36
- [35] Raabe O G 1968 *Amer. Indust. Hygiene Assoc. J.* **29** 439–443
- [36] Sheehan M J, Peters T M, Cena L, O’Shaughnessy P T and Gussman R A 2009 *Aerosol Sci. & Tech.* **43** 1091–1098
- [37] Ji J H, Bae G U, Yun S H, Jung J H, Noh A S and Kim S S 2007 *Aerosol Sci. & Tech.* **41** 786–793
- [38] Meuller B O, Messing M E, Engberg D L, Jansson A M, Johansson L I M, Norten S M, Tureson N and Deppart K 2012 *Aerosol Sci. & Tech.* **46** 1256–1270
- [39] Cho K, Chang H K, Kil D S, Park J H, Jang H D and Sohn H Y 2009 *Aerosol Sci. & Tech.* **43** 911–920
- [40] Chen D, Pui D H Y and Kaufman S I 1995 *J. Aerosol Sci.* **26** 963–977
- [41] Iida K, Sakurai H, Saito K and Ehara K 2014 *Aerosol Sci. & Tech.* **48** 789–802
- [42] Mitchell J P, Snelling K W and Stone R L 1987 *J. Aerosol Sci.* **18** 231–243
- [43] Wang J and Tronville 2014 *J. Nanopart. Res.* **16** 2417